ACES Asian Chemical Editorial Society

doi.org/10.1002/asia.202200296

CHEMISTRY AN ASIAN JOURNAL Research Article

www.chemasianj.org

Special Collection

Self-assembled Cupric Oxide Nanoclusters for Highly efficient chemodynamic therapy

Xinyu Jin,[a] Hongxia Zhao,[a] Zhicong Chao,[a] Xiaofeng Wang,[b] Qing Zhang,*[b] Huangxian Ju,[a] and Ying Liu*[a, c]

Abstract: Chemodynamic therapy (CDT) based on Fenton and Fenton-like reactions induces cancer cell killing via in situ catalyzing H_2O_2 and generating highly oxidative hydroxyl radicals (•OH) in tumor sites. Their application is not limited by tumor grown depth or hypoxic microenvironment. However, the reaction efficiency is still hampered due to the structure of catalytic agents and the requirement for low pH environment. Here, we design a porous CuO nanocluster (CuO NC) through self-assembly of oleylamine stabilized CuO NPs (OAm–CuO NPs), and functionalize it with folic acid (CuO NC-FA) for specific tumor cell targeting. It can catalyze H_2O_2 with high efficiency in nearly neutral environment. Besides, the porous structure of CuO NC also helps the diffusion of H_2O_2 to the interior of nanocluster to further improve Fenton-like reaction efficiency. The convenient synthesis of CuO NC-FA with good Fenton-like reaction efficiency at neutral environment demonstrates good chemodynamic therapy effect.

Introduction

Chemodynamic therapy that based on Fenton or Fenton-like reaction, which induces cancer cell killing via *in situ* generating highly oxidative hydroxyl radicals (•OH) in tumor sites, has become a promising treatment approach nowadays.[1] Metallic oxide[2] or metal-organic frameworks (MOF)[3] are common reactants to trigger Fenton or Fenton-like reaction with cancer cells highly expressed H_2O_2.[4] With the independence of extra light input or oxygen participation, the application of Fenton or Fenton-like reaction isn't limited by tumor grown depth or hypoxic microenvironment (TME).[5]

With Fe(II) as major catalyst, the reaction efficiency of Fenton reaction is vastly restricted by pH value of environment.[4] Considering the hydrolysis of Fe(II)/Fe(III) and corresponding generation of iron(oxy)hydroxide precipitation,[6] the optimal pH ranges for reaction is 2–4.[1,7] This doesn't fit for cytoplasm with close to neutral pH[8] as the expected place where Fenton reaction proceeds. Various efforts have been made to optimize Fenton or Fenton-like agents properties and modulate reaction environment in order to improve CDT effect.[1,9] Microwave showed a distinct advantage for penetration depth in tissues[10] and could be used to stimulate the Fenton/Fenton-like reaction.[11] Increasing the local electron density of Fe reaction center to improve kinetics of CDT[12] and developing amorphous iron nanoparticles to promote Fenton reaction in mildly acid tumor microenvironment were also effective approaches.[7] Intracellular H^+ accumulation strategy was also developed to meet the low pH requirement for Fe(II) based Fenton reaction,[5a] but it required complex nanoparticle design and the delivery of auxiliary agents which complicated the therapeutic process.[13] Cu(II) hydrolyzed species has higher solubility, and is also considered as a reactive species with H_2O_2.[14] Therefore, Cu(II) based nanomaterials are capable of efficient •OH production in close to neutral environment, which is an appropriate catalyst for Fenton-like reaction in cancer cells. However, it's difficult to control particle size, morphology, or obtain porous structure for currently reported CuO nanoparticles synthesized through hydrothermal method.[15] Therefore, Fenton-like reaction only proceeded at the surface of nanomaterial while inner part remained unreacted, which greatly limited •OH production efficiency.[16] CuS[17] and Copper-cysteamine[18] that directly synthesized in aqueous phase require external energy input, such as NIR light, UV irradiation, and low-dose MW excitation, to stimulate ROS generation for satisfactory therapeutic result. Precipitation on nanotemplate like SiO_2[15] or developing copper based MOF[19] could stabilize nanoparticle structure and increase Fenton-like reaction efficiency. However, the content of Cu(II), as the reactant for Fenton-like reaction, is low due to the existence of template or ligand molecule. Other therapeutic methods, such as photodynamic therapy, thus has to be applied along with Fenton-like reaction to improve therapeutic effect.[20] Therefore, novel nanostructure with high Cu(II) content and Fenton-like reaction efficiency is required.

[a] X. Jin, H. Zhao, Z. Chao, Prof. Dr. H. Ju, Prof. Dr. Y. Liu
State Key Laboratory of Analytical Chemistry for Life Science
School of Chemistry and Chemical Engineering
Nanjing University, Nanjing
210023 (P. R China)
E-mail: yingliu@nju.edu.cn

[b] X. Wang, Prof. Dr. Q. Zhang
Department of Urology
Affiliated Drum Tower Hospital
Medical School of Nanjing University
Institute of Urology, Nanjing University,
Nanjing 210008 (P. R. China)
E-mail: drzhangq@nju.edu.cn

[c] Prof. Dr. Y. Liu
Chemistry and Biomedicine Innovation Center
Nanjing University, Nanjing, 210023 (P. R. China)

Supporting information for this article is available on the WWW under https://doi.org/10.1002/asia.202200296

Special Collection This manuscript is part of a special collection highlighting Women in Chemistry.

CuO nanoparticles that synthesized in oil phase had controllable size with diameters below 5 nm through controlling the reaction time and temperature.[21] When self-assembled into nanocluster, the porous structure would result in large specific surface areas with high Cu content, which increased the active reaction sites and improved Fenton-like reaction efficiency. Herein, we synthesize CuO nanoclusters via self-assembling 5 nm sized CuO nanoparticles, and achieve highly efficient intracellular Fenton-like reaction with good •OH generation capability. Oleylamine stabilized CuO nanoparticles (OAm–CuO NPs) were synthesized and dispersed in cyclohexane.[22] Upon the addition of surfactant SDS, cyclohexane dispersed OAm–CuO NPs were self-assembled in oil-in-water micelle and concentrated into cluster structure with the evaporation of low-boiling cyclohexane (Scheme 1a). The as-obtained CuO nanoclusters (CuO NCs) were coated with SiO_2 shell, calcinated, and etched with NaOH solution. Subsequently, it was modified with folic acid (FA) for targeting cancer cells (Scheme 1b). The as-obtained CuO NCs-FA was delivered into HeLa cells to verify the feasibility of intracellular Fenton-like reaction (Scheme 1c). It demonstrated good reaction efficiency with •OH generation, cell killing capability and CDT effect. The convenient preparation of CuO NCs with good intracellular Fenton-like reaction efficiency at neutral environment had potential application in chemodynamic therapy.

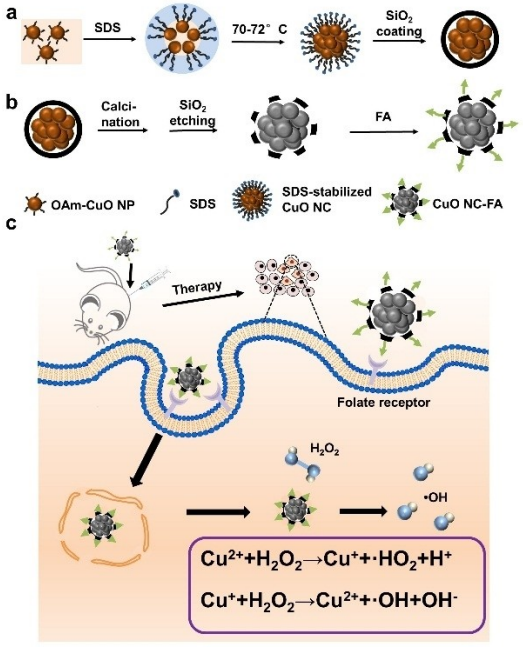

Scheme 1. Schematic illustration for synthesis of (a) CuO NCs and (b) CuO NCs-FA, (c) cellular uptake of CuO NCs-FA and intracellular Fenton-like reaction.

Results and Discussion

Synthesis and characterization of CuO nanoclusters (CuO NCs)

Oleylamine stabilized CuO nanoparticles (OAm–CuO NPs)[22] were synthesized and dispersed in cyclohexane. OAm–CuO NP was monodispersed with particle size of 5.5 ± 0.5 nm (Figure 1a). Both CuO (PDF#74-1021) and Cu_2O (PDF#05-0667) characteristic patterns were matched with X-ray diffraction (XRD) pattern of OAm–CuO NPs (Figure S1), indicating OAm–CuO NPs were composed of mixture of CuO and Cu_2O.

CuO NCs were fabricated through a temperature-controlled surfactant-assisted emulsion self-assembly method.[21a,23] The OAm–CuO NPs were dispersed in cyclohexane, with the addition of surfactant SDS aqueous solution and vortex / sonication, stable oil-in-water emulsion droplets were obtained. OAm–CuO NPs that confined in oil droplet were get concentrated and self-assembled into spherical clusters after evaporating cyclohexane (Scheme 1a).[21a,23] The as-obtained SDS stabilized CuO NCs were coated with a layer of SiO_2 and calcined at 400 °C in air, which removed organic ligands oleylamine and oxidized Cu_2O to CuO. The silica coating layer was then etched and obtained porous structured CuO NCs with diameter around 117 nm (Scheme 1b, Figure 1b), which kept good dispersion in water for several days.[21a] XRD pattern of CuO NCs matched well with the standard XRD pattern of CuO (PDF#74-1021) (Figure 1c), confirming the complete conversion of Cu_2O to CuO during calcination. X-ray photoelectron spectroscopy (XPS) showed that CuO NCs were mainly composed of Cu, O (Figure 1d), and demonstrate Cu $2p_{3/2}$ peak with corresponding satellite peaks at 934 eV and 943 eV, Cu $2p_{1/2}$ peak with corresponding satellite peak at 953 eV and 962 eV (Figure 1e).[24] The complete conversion of Cu_2O to CuO in nanocluster guaranteed the high reaction efficiency with H_2O_2 to generate •OH.[25] N_2 adsorption–desorption isotherm was used to evaluate the surface area of as-obtained particles (Figure 1f), and the Brunauer-Emmett-Teller (BET) surface area was 395.51 m^2/g for CuO NCs with porous structure and 7.92 m^2/g for aqueous dispersed CuO NPs (Aqu–CuO NPs).

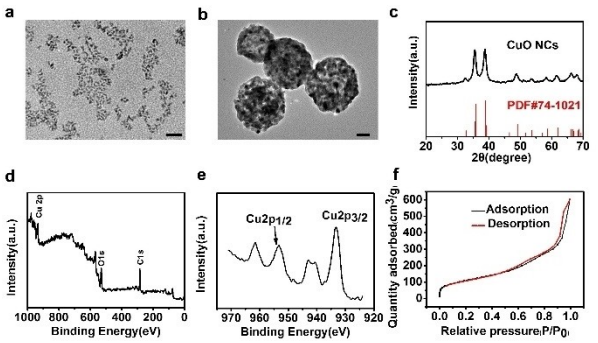

Figure 1. TEM characterizations of (a) OAm–CuO NPs. Scale bar: 20 nm and (b) CuO NCs. Scale bar: 25 nm. (c) XRD pattern of CuO NCs and standard pattern of CuO (PDF #74-1021). (d) XPS survey spectrum of CuO NCs and (e) high resolution Cu 2p spectrum of CuO NCs. (f) N_2 adsorption-desorption isotherm curves for self-assembled CuO NCs.

Fenton-Like Reaction of CuO NCs and in vitro •OH Generation

CuO NCs triggered Fenton-like reaction in the presence of cancer cell highly expressed H_2O_2 and generate •OH for cancer cell killing. Typical peak intensity of 1:2:2:1 for •OH radical was obviously observed on Electron spin resonance (EPR) spectroscopy with the co-existence of CuO NCs and H_2O_2 (Figure 2a, H_2O_2 + CuO NCs). CuO NCs or H_2O_2 alone didn't generate •OH (Figure 2a, H_2O_2, CuO NCs). •OH oxidizes methylene blue (MB) from blue to colorless, therefore the decrease of MB characteristic absorbance at 664 nm was measured to evaluate •OH generation. With fixed H_2O_2 concentration of 4 mM, MB characteristic absorption peak demonstrated gradual decrease corresponding to CuO NCs concentration from 10–60 μg/mL (Figure 2b). MB degradation was also dependent on H_2O_2 concentration with CuO NCs concentration fixed at 40 μg/mL, which showed 16.7% of MB degradation with 0.1 mM H_2O_2 and almost complete MB degradation with 6 mM H_2O_2 (Figure 2c). Terephthalic acid (TPA), which reacts with •OH and produces fluorescent 2-hydroxyterephthalic acid, was also used to verify •OH generation. It also demonstrated gradual increase of 2-hydroxyterephthalic acid characteristic emission peak at 435 nm corresponding to CuO NCs concentration from 10–50 μg/mL (Figure S2a) and H_2O_2 concentration from 0.1–6 mM (Figure S2b).

pH effect on Fenton-like reaction efficiency was evaluated by measuring MB absorbance respectively after 1-hour reaction at different pH from 4.0–10.0. Unlike iron ions based Fenton reaction that required for strong acidic environment (pH 2.0–4.0) due to the generation of undesired ferric oxyhydroxides as pH increased,[6a] CuO NCs showed best catalytic efficiency at close to neutral environment at pH 7.0 (Figures S2c) with maximum MB characteristic peak suppression of 84.3% (Figure 2d). Time dependent absorbance decrease at 664 nm was also monitored at pH 5.0, 6.5, 7.4, which showed obvious slower MB degradation at pH 5.0, further confirming the efficient •OH production in neutral and weak acidic environments (Figure S3). There are more redundant H^+ to react with •OH in lower pH.[25a26] This means the generated reactive •OH radicals would be consumed, ultimately hinders •OH production efficiency in lower pH. Therefore, close to neutral environment of cytoplasm[8] promotes the reaction efficiency of CuO NCs based Fenton-like reaction. Various Cu-based nanomaterials, including CuO,[27] have been used as heterogeneous Fenton-like catalysts.[11,18] They had higher reaction rate with H_2O_2 than Fe-based nanomaterials and showed excellent Fenton-like catalytic activity at neutral pH. The Fenton-like reaction can be represented by Eqs.(1) and (2).

$$Cu^{2+} + H_2O_2 \rightarrow Cu^{+} + {}^{\bullet}HO_2 + H^{+} \quad (1)$$

$$Cu^{+} + H_2O_2 \rightarrow Cu^{2+} + {}^{\bullet}OH + OH^{-} \quad (2)$$

To evaluate the contribution of porous structure to CuO NCs Fenton-like reaction, aqueous dispersed CuO NPs (Aqu–CuO NPs) were synthesized through hydrothermal method.[15] Aqu–CuO NPs demonstrated similar XRD pattern (Figure S4a) and XPS spectra (Figure S4b, c) as CuO NCs, but obvious nonporous structure (Figure S4d) and smaller BET surface area of 7.92 m^2/g. Different concentration of CuO NCs and Aqu–CuO NPs were incubated with MB and 1 mM H_2O_2 at pH 6.5 for 2 h, CuO NCs resulted in much more obvious decreased of MB characteristic absorbance peak compared with Aqu–CuO NPs (Figure S5a, b). H_2O_2 concentrations in supernatants after reaction were also quantified with H_2O_2 detection kit, and obtained 0.62 ± 0.03 mM for Aqu–CuO reaction group and 0.29 ± 0.01 mM for CuO–NCs reaction group (Figure S5c). The porous structure of CuO–NCs improved reaction efficiency with H_2O_2. Therefore, the porous structure of CuO NCs not only increased surface area, but also prompted diffusion of H_2O_2 into the interior of nanocluster, which enhanced the reaction efficiency of Fenton-like reaction.

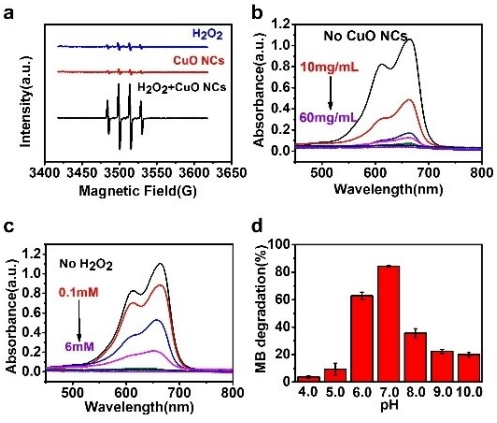

Figure 2. (a) EPR spectra of H_2O_2, CuO NCs, and the mixture of H_2O_2 and CuO NCs (H_2O_2 + CuO NCs) with DMPO as •OH trapping agent. UV-Vis absorption spectra of MB corresponding to (b) 10, 20, 30, 40, 50, 60 μg/mL CuO NCs with H_2O_2 concentration fixed at 4 mM and (c) 0.1, 0.5, 1, 2, 4, 6 mM H_2O_2 with CuO NCs concentration fixed at 40 μg/mL. (d) Degradation percentage of MB characteristic absorbance at 664 nm at different pH. The error bars indicate means ± S.D. (n = 3)

Intracellular delivery of CuO NCs

To facilitate specific cancer cell delivery, CuO NCs surface was functionalized with folic acid to target cancer cells. CuO NCs were dispersed in APTES ethanol solution and stirred overnight to modify –NH_2, the obtained CuO NCs-NH_2 were then modified with NHS-PEG-FA via amide bonds. The functionalization of FA was confirmed by FTIR spectrum, CuO NCs-FA demonstrated FA characteristic peaks at 1190 cm^{-1} for C–N stretching vibration, 1695 cm^{-1} and 1641 cm^{-1} for C=O stretching vibration of carboxyl group and –CONH– group respectively (Figure 3a). Ninhydrin, which reacts with amino group to produce blue-purple compound with characteristic absorbance at 570 nm, was used to titrate the stoichiometry of –NH_2 on CuO NCs and CuO NCs-FA respectively. The number of FA was calculated as 1293 ± 104 per particle by comparing NH_2 numbers before and after FA conjuation (Figure S6). The zeta potential of CuO NCs increased from 9.13 ± 0.47 mV to 11.97 ± 0.06 mV after NH_2 functionalization (CuO NCs–NH_2), and decreased to 5.16 ±

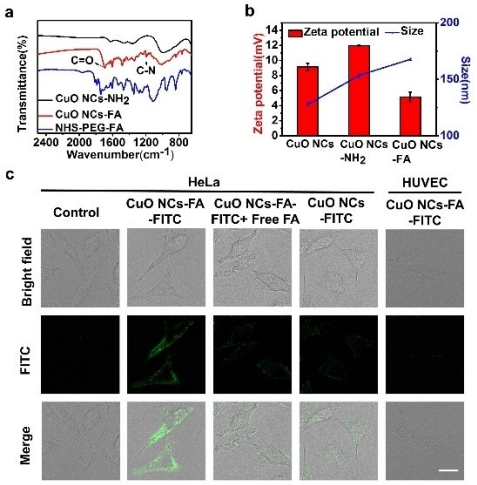

Figure 3. (a) FT-IR spectra of CuO NCs-NH_2, CuO NCs-FA, NHS-PEG-FA. (b) zeta potential and DLS of CuO NCs, CuO NCs-NH_2, CuO NCs-FA. (c) CLSM images of HeLa cell incubated with CuO NCs-FA-FITC, FA pretreated HeLa cells incubated with CuO NCs-FA-FITC (CuO NCs-FA-FITC + free FA), HeLa cells incubated with CuO NCs-FITC and HUVEC cells incubated with CuO NCs-FA-FITC. Scale bar = 30 μm.

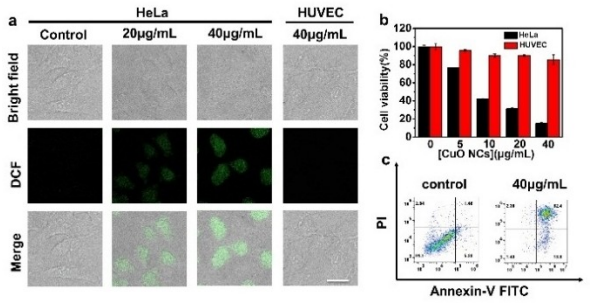

Figure 4. (a) DCF fluorescence images of HeLa cells incubated with 20 μg/mL and 40 μg/mL of CuO NCs-FA and HUVEC cells with 40 μg/mL of CuO NCs-FA. Scale bar = 30 μm. (b) Cell viability of HeLa and HUVEC cells incubated with 5, 10, 20, 40 μg/mL of CuO NCs-FA respectively for 24 h. The error bars indicate means ± S.D. (n = 3). (c) Flow cytometry detection of apoptotic HeLa cells after 24 h of treatment with CuO NCs-FA.

0.63 mV after modification of NHS-PEG-FA (Figure 3b). The DLS of CuO NCs increased from 127.72 nm to 167.74 nm after the modification of NHS-PEG-FA (Figure 3b). With high expression level of folic acid receptor on cell membrane,[28] HeLa cells were chosen as model cell to demonstrate the intracellular delivery of CuO NCs-FA. CuO NCs-FA was modified with FITC (CuO NCs-FA-FITC) and incubated with HeLa cells, which demonstrated clear intracellular FITC fluorescence in cytoplasm after 4 hours incubation (Figure 3c, CuO NCs-FA-FITC), indicating the successful internalization of CuO NCs-FA-FITC. In comparison, FITC fluorescence was barely observed from HeLa cells incubated with CuO NCs-FITC (Figure 3c, CuO NCs-FITC), free FA pretreated HeLa cells incubated with CuO NCs-FA-FITC (Figure 3c, CuO NCs-FA-FITC + free FA) and HUVEC cells incubated with CuO NCs-FA-FITC (Figure 3c, HUVEC). This result indicated good FA receptor based tumor cell targeting capability of CuO NCs-FITC.

Intracellular •OH generation and therapeutic effect

2′,7′-dichlorodihydrofluorescein diacetate (DCFH-DA), which is oxidized by ROS to generate 2′,7′-dichlorofluorescein (DCF) with green fluorescence, was used to evaluate intracellular ROS generation. CuO NCs-FA incubated HeLa cells demonstrated obvious intracellular DCF fluorescence, whose intensity was increased with incubated CuO NCs-FA concentrations (Figure 4a). CuO NCs-FA incubated HUVEC cells barely showed intracellular DCF fluorescence (Figure 4a, HUVEC). Intracellular •OH generation was also confirmed by incubating TPA with HeLa cells digest that treated with CuO NCs-FA (Figure S5d, CuO NCs-FA), which demonstrated about 2.53 times fluorescence intensity compared with HeLa cells digest in the absence of CuO NCs-FA treatment (Figure S5d, control). This result confirmed efficient and specific intracellular ROS generation.

The therapeutic effect of intracellular Fenton reaction was evaluated by 3-(4,5-dimethylthiazol-2-yl)-2-diphenyltetrazolium bromide (MTT) assay. CuO NCs-FA showed enhanced cytotoxicity to HeLa cells according to dose, and the cell viability dropped to only 15.3% with 40 μg/mL CuO NCs-FA (Figure 4b). This result demonstrated good therapeutic effect of CuO NCs-FA at cellular level. CuO NCs-FA also showed good biocompatibility with little cytotoxicity to normal cells. The cell viability was 85.5% for 40 μg/mL CuO NCs-FA incubated normal cell HUVEC cells (Figure 4b). Live/dead cell staining assay also showed HeLa cell death in a dose-dependent manner of CuO NCs-FA (Figure S7). Cell apoptosis was further assessed by flow cytometry. Substantial higher percentage of apoptotic cells was detected in CuO NCs-FA treated HeLa cells (Figure 4c). The elevation of intracellular •OH resulted in higher cell apoptosis, and would have potential contribution to Fenton like-reaction based therapy.

In vivo CDT effect

The *in vivo* CDT effect of CuO NCs-FA was verified with subcutaneous HeLa tumor mouse model. CuO NCs-FA injected mice group demonstrated obvious suppression of tumor growth compared with saline injected mice group (Figure 5a, b). Both the CuO NCs-FA injected mice group and saline injected mice group demonstrated no apparent decline of body weight during 14 days of observation (Figure 5c), indicating good biocompatibility of CuO NCs-FA. H&E staining demonstrated more severe cell necrosis/ apoptosis for tumor tissue from CuO NCs-FA injected mice group compared with saline injected mice group (Figure 5d, Tumor). CuO NCs-FA injection barely affected other organs compared with saline injected group (Figure 5d, Heart, liver, spleen, lung, kidney). These results verified the specificity and feasibility of CuO NCs-FA for cancer therapy.

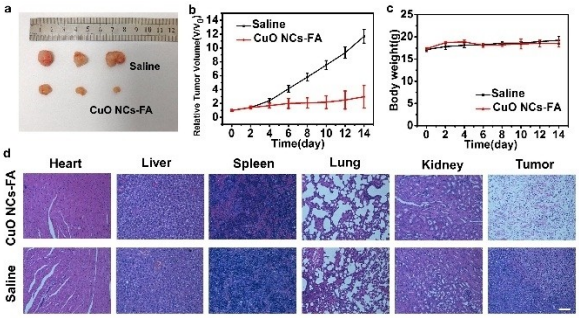

Figure 5. (a) Photos of tumors at 14th day of treatment, (b) relative tumor growth curves, (c) time-dependent body-weight curves and (d) H&E-stained slices of tumor and major organs after therapy for CuO NCs-FA injected mice group and saline injected mice group. The error bars in b) and c) indicate means ± S.D. (n = 3). Scale bar = 100 μm.

Conclusion

In this work, a novel nanoagent for high efficient CDT was developed. CuO nanoclusters (CuO NCs) were fabricated through self-assembled OAm–CuO nanoparticles, which had porous structure and favored the diffusion of H_2O_2 as Fenton-like reaction reactant to the interior of the nanocluster. Notably, optimal Fenton-like reaction was achieved under nearly neutral environment, which was beneficial to the significant generation of •OH in tumor cells. Overall, we expect that this work will provide new insight into the future development of CDT.

Experimental Section

Materials and Reagents

Sodium dodecyl sulfate (SDS), 1-octadecene (ODE) and oleylamine were purchased from Sigma-Aldrich (USA). Cupric acetate monohydrate, acetone, sodium hydroxide, cyclohexane, ethanol, ammonium hydroxide solution (NH_4OH, ~28% NH_3 in water), N, N′-dimethylformamide (DMF), tetraethyl orthosilicate (TEOS), (3-aminopropyl) triethoxysilane (APTES), terephthalic acid (TPA) and methylene blue were purchased from Aladdin Ltd (Shanghai, China). NHS-PEG-folic acid (NHS-PEG-FA) (MW 2000) was purchased from Toyongbio (Shanghai, China). 4-dimethylaminopyridine (DMAP) was purchased from Adamas Reagent, Ltd. (Shanghai, China). DCFH-DA, Dulbecco's modified Eagle's medium (DMEM), RPMI-1640 medium, PBS, fetal bovine serum (FBS), Calcein-AM/PI Double Stain Kit, Annexin V-fluorescein isothiocyanate (FITC)/propidium iodide (PI) apoptosis detection kit and 3-(4,5-dimethylthiazol-2-yl)-2-diphenyltetrazolium bromide (MTT) detection kit, human cervical carcinoma cell line (HeLa) and human umbilical vein endothelial cell line (HUVEC) were purchased from Keygen Biotech (Nanjing, China).

Characterization

Transmission electron microscopic (TEM) images were acquired on JEM-2100 transmission electron microscope (JEOL Ltd., Japan). Dynamic light scattering was performed on a Zeta Plus 90 Plus/BI-MAS (Brook haven, USA). Powder X-ray diffraction (XRD) analysis was performed on ARL X'TRA XRD system (Thermo Fisher Scientific, USA). X-ray photoelectron spectroscopy (XPS) was performed on Thermo ESCALAB 250XI (Thermo-Fisher, United States). Nitrogen (N_2) adsorption desorption isotherm curves were obtained using a TriStar 3000 (Micromeritics, Norcross, GA, USA) surface area analyzer. UV–Vis absorption spectra were recorded with Nanodrop-2000 C UV-Vis spectrophotometer (Nanodrop, USA). Fluorescence spectra were recorded with F-7000 Spectro fluorophotometer (HITACHI, Japan). MTT assays were conducted on Hitachi/Roche System Cobas 6000 (Bio-Rad, USA). Flow cytometric analysis was conducted on a Coulter FC-500 flow cytometer (Beckman – Coulter, USA). Confocal fluorescence images were taken with a TCS SP8 confocal laser scanning microscope (Leica, Germany).

Synthesis of Oleylamine stabilized CuO nanoparticles (OAm–CuO NPs)

Oleylamine stabilized CuO nanoparticles that dispersed in organic solvent were synthesized referred to a previously reported method.[22] Briefly, 3 mmol cupric acetate monohydrate was dissolved in a mixture of 30 mL ODE and 18 mL oleylamine. The mixtures were kept stirring and heating to 120 °C in vacuum, and continuously reacted at 120 °C until the solution turned to dark brown. The as-obtained OAm–CuO NPs were washed with cyclohexane and acetone several times, and re-dispersed in cyclohexane for further use.

In comparison, aqueous dispersed CuO NPs (Aqu–CuO NPs) were also synthesized via hydrothermal method.[15] 0.8 mmol cupric acetate monohydrate was dispersed in 35 mL H_2O to form a transparent blue solution. 0.5 M NaOH solution was then added in until the solution turned dark blue. The as-obtained solution was vigorously stirred for 30 min, and transferred into a Teflon lined stainless steel autoclave, which was heated to 180 °C and maintained for 6 h. Aqu–CuO NPs were obtained as a black product by centrifugation and washed several times with water.

Synthesis of CuO nanoclusters (CuO NCs)

CuO NCs were synthesized through a temperature-controlled surfactant-assisted emulsion self-assembly method.[21a] 1 mL of the above obtained OAm–CuO NPs that dispersed in cyclohexane was well mixed with 10 mL aqueous solution of SDS to get CuO–SDS micelles, kept stirring and heating to 70 –72 °C in a water bath for 4 hours to evaporate cyclohexane. The as-obtained CuO NCs were washed with water and re-dispersed in water.

Surface functionalization of CuO NCs

CuO NCs aqueous dispersed solution was mixed with 1 mL ammonium hydroxide solution and 20 mL ethanol under stirring. 20 μL TEOS was then added in and reacted for 20 minutes. After centrifugation and washing, the precipitates were dried overnight and heated to 400 °C for 2 hours in air to remove organic agents. The as-obtained silica shell coated CuO NCs were stirred in 0.5 M NaOH solution, washed with 0.1 M acetic acid solution and water for several times, and reacted with APTES ethanol solution overnight for surface functionalization of -NH_2 group. The as-obtained CuO NCs-NH_2 was washed with ethanol for three times, and re-dispersed in DMF.

1 mg/mL the above-obtained CuO NCs-NH_2 were subsequently mixed with 1% NHS-PEG-FA and 0.1 mg/mL DMAP DMF solution, kept stirring for 12 h in dark at room temperature, and centrifuged to get folic acid functionalized CuO NCs (CuO NCs-FA). The as-obtained CuO NCs-FA were centrifuged, washed with DMF and PBS for three times, and re-dispersed in PBS for future use.

In vitro verification of ·OH generation

The decrease of MB characteristic absorbance peak at 664 nm was measured to evaluate •OH generation. To evaluate the effect of CuO NCs-FA on •OH generation efficiency, different concentrations of CuO NCs-FA (10, 20, 30, 40, 50, 60 μg/mL) was added in 10 μg/mL MB PBS (pH = 6.5) solution containing 4 mM H_2O_2 respectively, and incubated at 37 °C for 2 hours. To evaluate the effect of H_2O_2 on •OH generation efficiency, a similar experiment was performed by mixing 10 μg/mL MB PBS (pH = 6.5) solution containing 40 μg/mL CuO NCs-FA with different concentrations of H_2O_2 (0.1, 0.5, 1, 2, 4, 6 mM). To evaluate the effect of pH on •OH generation efficiency, 40 μg/mL CuO NCs-FA and 4 mM H_2O_2 were mixed with 10 μg/mL MB PBS with different pH (from 4.0 to 10.0), reacted at 37 °C for 1 h. The absorbance of the mixture solutions were also recorded along with time for reaction conditions of pH = 5.0, 6.5 and 7.4.

As the reaction product of •OH oxidized TPA, fluorescence of 2-hydroxyterephthalic acid at 435 nm was further measured to evaluate •OH generation. Different concentrations of CuO NCs-FA (10, 20, 30, 40, 50 μg/mL) were added in TPA PBS (pH = 6.5) containing 4 mM H_2O_2, reacted for 2 hours, and the characteristic fluorescence peak at 435 nm was recorded. Similarly, different concentrations of H_2O_2 (0.1, 0.5, 1, 2, 4, 6 mM) were added in TPA PBS (pH = 6.5) containing 40 μg/mL CuO NCs-FA, reacted for 2 hours, and the characteristic fluorescence peak at 435 nm was recorded.

EPR was also used to conform ·OH generation with DMPO as the spin trapping agent. 500 μM H_2O_2 in PBS (pH = 6.5), 40 μg/mL CuO NCs-FA in PBS (pH = 6.5), and the mixture of 500 μM H_2O_2 and 40 μg/mL CuO NCs-FA in PBS (pH = 6.5) were incubated at 37 °C for 30 minutes respectively. 50 μL 10 mM DMPO was then added and transferred the solution into a quartz capillary using capillarity for EPR spectrometry measurement.

Ninhydrin reaction

Lithium acetate dihydrate and acetic acid were dissolved in DI water to get lithium acetate buffer solution (4 M, pH = 5.2). Ninhydrin (160 mg) and hydrindantin (24 mg) were mixed in 6 mL of 2-methoxyethanol, and 1 mL of lithium acetate solution was subsequently added in to get ninhydrin solution. 100 μL standard solution or titrating sample, 100 μL lithium acetate, and 100 μL ninhydrin solution were mixed together and boiled in water at 100 °C for 12 min. After cooling down to room temperature, 200 μL of ethanol/water mixed solution (1 : 1, v/v) was added in with the subsequent absorption spectra measurement.

Cell culture

Human cervical carcinoma (HeLa) cells and Human Umbilical Vein Endothelial Cells (HUVEC) were cultured in DMEM containing 10% FBS and 1% penicillin/streptomycin at 37 °C in a humidified atmosphere with 5% CO_2.

Cellular Uptake Characterizations

HeLa cells were seeded in a confocal dish, incubated at 37 °C for 24 h, the medium was then replaced by fresh DMEM containing 40 μg/mL FITC-labeled CuO NCs-FA (CuO NCs-FA-FITC). After different incubation times (0, 4 h), the treated cells were washed with phosphate-buffered saline (PBS), then the fluorescence signals were collected from 500 to 550 nm. Besides, CuO NCs-FA-FITC were incubated with cells pretreated with 1 mM FA, CuO NCs-FITC without FA modification were incubated with HeLa cells for comparison. Furthermore, the same operation was performed on HUVEC with incubation of CuO NCs-FA-FITC.

Cytotoxicity measurement

HeLa/ HUVEC cells were seeded in 96-well microplates (1×10^4 cells per well) and cultured overnight. The cell culture medium was then replaced by fresh DMEM containing different concentrations of CuO NCs-FA (0, 5, 10, 20, 40 μg/mL). After continuous incubation for 24 h, 50 μL MTT solution was added to each well individually and incubated for another 4 h. The cell culture medium was then replaced with 150 μL DMSO to dissolve the crystal precipitates. The cell viability was determined by measuring the solution absorbance at 490 nm and estimated according to the following equation: Cell viability (%) = $(A_{test}/A_{control}) \times 100\%$.

Intracellular verification of ROS generation

DCFH-DA was used as a fluorescent ROS probe to image intracellular •OH generation. HeLa cells were cultured with different concentrations of CuO NCs-FA (0, 20, 40 μg/mL) for 4 h. The cell culture medium was then replaced with fresh DMEM containing 10 μM DCFH-DA and continuously incubated for another 30 min. After washing with PBS for 3 times, DCF signal was observed using CLSM under 488 nm excitation. As a comparison, the same operation was performed on HUVEC cells with 40 μg/mL CuO NCs-FA.

HeLa cells were incubated with 100 μM H_2O_2 and 40 μg/mL CuO NCs-FA for 4 h, then digested and dispersed in 1 mL PBS contained 5 mM TPA (about 1.3×10^7 cells/mL). HeLa cells that were not treated with CuO NCs-FA were set as control. The fluorescence spectra of TPA were recorded.

Live/Dead cells staining

The effect of Fenton-like reaction effect to HeLa cells was evaluated by Calcein AM/PI live/dead staining. HeLa cells were incubated with different concentrations of CuO NCs-FA (0, 20, 40 μg/mL) for 12 h, washed twice with PBS, and stained with Calcein-AM and PI solution for 30 min. CLSM images were then recorded after washing the cells with PBS.

Cell apoptosis analysis

Cell apoptosis induced by CuO NCs-FA was analyzed by flow cytometry. HeLa cells were seeded in 6-well plates and adhered overnight, subsequently incubated with 40 μg/mL CuO NCs-FA for 24 h, collected and washed twice with PBS. The as-obtained cells were then stained with 5 μL Annexin V-FITC and 5 μL PI for 5 min in the dark, and detected with flow cytometry.

In vivo CDT effect

All experimental processes were consistent with the Institutional Animal Use and Care Regulations approved by the Model Animal Research Center of Nanjing University (MARC) with the permit number for animal usage of SYXK(SU)2019-0056. All mice used in this work were purchased from Pusheng Biomedical Biotech. Co., Ltd. (Nanjing, China). The tumor models were established by subcutaneous injection of HeLa cells (1.0×10^7 cells/mL) into the armpit of female BALB/c nude mice. When the tumor sizes reached about 70–90 mm^3, the mice were randomly divided into two groups (3 mice in each group). Mice groups were intratumorally injected

with 150 μL of saline or CuO NCs-FA (0.5 mg/mL) respectively. The tumor sizes and body weights were recorded every other day for 14 days of therapeutic treatment. After 14 days of observation, the mice were sacrificed for histological analysis.

Acknowledgements

We gratefully acknowledge the National Natural Science Foundation of China (21974064, 22022405), Natural Science Foundation of Jiangsu Province for distinguished Young Scholars (BK20200010).

Conflict of Interest

The authors declare no conflict of interest.

Data Availability Statement

The data that support the findings of this study are available from the corresponding author upon reasonable request.

Keywords: Fenton-like reaction · CuO nanocluster · Self-assembly

[1] Z. Tang, Y. Liu, M. He, W. Bu, *Angew. Chem. Int. Ed.* **2019**, *58*, 946–956; *Angew. Chem.* **2019**, *131*, 958–968.
[2] a) M. Y. Zhang, X. J. Liu, Q. Luo, Q. Wang, L. J. Zhao, G. Y. Deng, R. B. Ge, L. Zhang, J. Q. Hu, J. Lu, *Chem. Eng. J.* **2020**, *389*,124450; b) S. S. Gao, H. Lin, H. X. Zhang, H. L. Yao, Y. Chen, J. L. Shi, *Adv. Sci.* **2019**, *6*, 1801733.
[3] a) S. Liang, X. Xiao, L. X. Bai, B. Liu, M. Yuan, P. A. Ma, M. L. Pang, Z. Y. Cheng, J. Lin, *Adv. Mater.* **2021**, *33*, 2100333; b) Y. Ding, H. Xu, C. Xu, Z. R. Tong, S. T. Zhang, Y. Bai, Y. N. Chen, Q. H. Xu, L. Z. Zhou, H. Ding, Z. Q. Sun, S. Yan, Z. W. Mao, W. L. Wang, *Adv. Sci.* **2020**, *7*, 2001060.
[4] Y. Liu, W. Zhen, Y. Wang, J. Liu, L. Jin, T. Zhang, S. Zhang, Y. Zhao, S. Song, C. Li, J. Zhu, Y. Yang, H. Zhang, *Angew. Chem. Int. Ed.* **2019**, *58*, 2407–2412; *Angew. Chem.* **2019**, *131*, 2429–2434.
[5] a) X. Y. Chen, H. L. Zhang, M. Zhang, P. R. Zhao, R. X. Song, T. Gong, Y. Y. Liu, X. H. He, K. L. Zhao, W. B. Bu, *Adv. Funct. Mater.* **2020**, *30*,1908365 ; b) S. Y. Fu, R. H. Yang, L. Zhang, W. W. Liu, G. Y. Du, Y. Cao, Z. G. Xu, H. J. Cui, Y. J. Kang, P. Xue, *Biomaterials* **2020**, *257*, 120279; c) C. Zhang, W. Bu, D. Ni, S. Zhang, Q. Li, Z. Yao, J. Zhang, H. Yao, Z. Wang, J. Shi, *Angew. Chem. Int. Ed.* **2016**, 55, 2101–2106; *Angew. Chem.* **2016**, *128*, 2141–2146.
[6] a) J. J. Pignatello, E. Oliveros, A. MacKay, *Crit. Rev. Environ. Sci. Technol.* **2007**, 37, 273–275; b) K. Fuku, H. Kanai, M. Todoroki, N. Mishima, T. Akagi, T. Kamegawa, N. Ikenaga, *Chem. Asian J.* **2021**, *16*, 1887–1892.
[7] Y. W. Kang, K. Y. Hwang, *Water Res.* **2000**, *34*, 2786–2790.
[8] O. Tredan, C. M. Galmarini, K. Patel, I. F. Tannock, *J. Natl. Cancer Inst.* **2007**, *99*, 1441–1454.
[9] a) Z. M. Tang, P. R. Zhao, H. Wang, Y. Y. Liu, W. B. Bu, *Chem. Rev.* **2021**, *121*, 1981–2019; b) J. H. Ma, W. H. Ma, C. C. Chen, H. W. Ji, J. C. Zhao, *Chem. Asian J.* **2011**, *6*, 2264–2268.
[10] a) N. K. Pandey, W. Xiong, L. Y. Wang, W. Chen, B. Bui, J. Yang, E. Amador, M. L. Chen, C. Xing, A. A. Athavale, Y. W. Hao, W. Feizi, L. Lumata, *Bioact. Mater.* **2021**, *7*, 112–125; b) X. Chu, K. Li, H. Y. Guo, H. B. Zheng, S. Shuda, X. L. Wang, J. Y. Zhang, W. Chen, Y. Zhang, *ACS Biomater. Sci. Eng.* **2017**, *3*, 1836–1844; c) M. Y. Yao, L. Ma, L. H. Li, J. Y. Zhang, R. X. Lim, W. Chen, Y. Zhang, *J. Biomed. Nanotechnol.* **2016**, *12*, 1835–1851.
[11] N. K. Pandey, H. B. Li, L. Chudal, B. Bui, E. Amador, M. B. Zhang, H. M. Yu, M. L. Chen, X. Luo, W. Chen, *Mater. Today Phys.* **2022**, *22*, 100587.
[12] P. R. Zhao, Y. Q. Jiang, Z. M. Tang, Y. L. Li, B. X. Sun, Y. L. Wu, J. Y. Wu, Y. Y. Liu, W. B. Bu, *Angew. Chem. Int. Ed.* **2021**, *60*, 8905–8912.
[13] Y. L. Liu, X. Y. Ji, W. W. L. Tong, D. Askhatova, T. Y. Yang, H. W. Cheng, Y. Z. Wang, J. J. Shi, *Angew. Chem. Int. Ed.* **2018**, *57*, 1510–1513; *Angew. Chem.* **2018**, *130*, 1526–1529.
[14] a) F. J. Millero, R. L. Johnson, C. A. Vega, V. K. Sharma, S. Sotolongo, *J. Solution Chem.* **1992**, *21*, 1271–1287; b) K. C. Liang, H. T. Sun, Z. B. Yang, H. Z. Yu, J. Shen, X. L. Wang, H. R. Chen, *Adv. Funct. Mater.* **2021**, *31*, 2100355.
[15] M. D. Sun, D. Yang, Q. Q. Sun, T. Jia, Y. Kuang, S. L. Gai, F. He, F. M. Zhang, P. P. Yang, *J. Mater. Chem. B* **2020**, *8*, 10559–10576.
[16] Z. M. Tang, H. L. Zhang, Y. Y. Liu, D. L. Ni, H. Zhang, J. W. Zhang, Z. W. Yao, M. Y. He, J. L. Shi, W. B. Bu, *Adv. Mater.* **2017**, *29*,1701683.
[17] L. H. Li, L. H. Rashidi, M. Y. Yao, L. Ma, L. L. Chen, J. Y. Zhang, Y. Zhang, W. Chen, *Photodiagn. Photodyn. Ther.* **2017**, *19*, 5–14.
[18] N. K. Pandey, L. Chudal, J. Phan, L. W. Lin, O. Johnson, M. Y. Xing, J. P. Liu, H. B. Li, X. J. Huang, Y. Shu, W. Chen, *J. Mater. Chem. B.* **2019**, *7*, 6630–6642.
[19] D. D. Wang, H. H. Wu, C. L. Wang, L. Gu, H. Z. Chen, D. Jana, L. L. Feng, J. W. Liu, X. Y. Wang, P. P. Xu, Z. Guo, Q. W. Chen, Y. L. Zhao, *Angew. Chem. Int. Ed.* **2021**, *60*, 3001–3007; *Angew. Chem.* **2021**, *133*, 3038–3044.
[20] S. Wang, G. C. Yu, W. J. Yang, Z. T. Wang, O. Jacobson, R. Tian, H. Z. Deng, L. S. Lin, X. Y. Chen, *Adv. Sci.* **2021**, *8*, 2002927.
[21] a) Z. D. Lu, M. M. Ye, N. Li, W. W. Zhong, Y. D. Yin, *Angew. Chem. Int. Ed.* **2010**, *49*, 1862–1866; *Angew. Chem.* **2010**, *122*, 1906–1910; b) F. Bai, D. S. Wang, Z. Y. Huo, W. Chen, L. P. Liu, X. Liang, C. Chen, X. Wang, Q. Peng, Y. D. Li, *Angew. Chem. Int. Ed.* **2007**, *46*, 6650–6653; *Angew. Chem.* **2007**, *119*, 6770–6773.
[22] a) W. Jia, Y. X. Liu, P. F. Hu, R. Yu, Y. Wang, L. Ma, D. S. Wang, Y. D. Li, *Chem. Commun.* **2015**, *51*, 8817–8820; b) X. W. Liu, B. Y. Geng, Q. B. Du, J. Z. Ma, X. M. Liu, *Mat. Sci. Eng. A-Struct.* **2007**, *448*, 7–14.
[23] Z. Zhang, M. K. G. Jayakumar, X. Zheng, S. Shikha, Y. Zhang, A. Bansal, D. J. J. Poon, P. L. Chu, E. L. L. Yeo, M. L. K. Chua, S. K. Chee, Y. Zhang, *Nat. Commun.* **2019**, *10*, 4586.
[24] L. S. Lin, T. Huang, J. B. Song, X. Y. Ou, Z. T. Wang, H. Z. Deng, R. Tian, Y. J. Liu, J. F. Wang, Y. Liu, G. C. Yu, Z. J. Zhou, S. Wang, G. Niu, H. H. Yang, X. Y. Chen, *J. Am. Chem. Soc.* **2019**, *141*, 9937–9945.
[25] a) J. K. Kim, I. S. Metcalfe, *Chemosphere* **2007**, *69*, 689–696; b) H. S. Wu, F. H. Chen, C. Q. You, Y. Zhang, B. W. Sun, Q. Zhu, *Small* **2020**, *16*, 2001805.
[26] M. S. Zhang, X. L. Wang, *ACS Omega* **2021**, *6*, 18414–18425.
[27] S. Sehati, M. H. Entezari, *Appl. Surf. Sci.* **2017**, *399*, 732–741.
[28] S. Bettini, G. Giancane, R. Pagano, V. Bonfrate, L. Salvatore, M. Madaghiele, A. Buccolieri, D. Manno, A. Serra, G. Maruccio, A. G. Monteduro, Z. Syrgiannis, L. Valli, M. Prato, *J. Mater. Chem. B* **2017**, *5*, 7547–7556.

Manuscript received: March 23, 2022
Revised manuscript received: June 4, 2022
Accepted manuscript online: June 17, 2022
Version of record online: June 30, 2022